Chemistry & Biodiversity

WILEY-VCH

CHEMISTRY & BIODIVERSITY

RESEARCH ARTICLE

Toward a Better Understanding of Fatty Acid Amide Hydrolase Inhibition by β-Lactams

Axel Morelle[1,2] | Juhans Dechenne[1] | Joséphine Caruano[1] | Olivia Vander Auwera[1] | Gabriella Barozzino-Consiglio[1] | Catherine Michaux[3] | Giulio G. Muccioli[2] | Raphaël Robiette[1]

[1]Institute of Condensed Matter and Nanosciences, Université catholique De Louvain, Louvain-la-Neuve, Belgium | [2]Bioanalysis and Pharmacology of Bioactive Lipids Research Group, Louvain Drug Research Institute, Université catholique De Louvain, Brussels, Belgium | [3]Namur Institute of Structured Matter (NISM) Namur Research Institute for Life Sciences (NARILIS), Laboratoire de Chimie Physique Des Biomolécules, Université de Namur, Namur, Belgium

Correspondence: Catherine Michaux (catherine.michaux@unamur.be) | Giulio G. Muccioli (giulio.muccioli@uclouvain.be) | Raphaël Robiette (raphael.robiette@uclouvain.be)

Received: 17 September 2025 | **Revised:** 27 October 2025 | **Accepted:** 28 October 2025

Keywords: β-lactam | FAAH | Inhibitor

ABSTRACT

Fatty acid amide hydrolase (FAAH) inhibition holds therapeutic promise by enhancing endocannabinoid signaling. We previously identified β-lactam compounds as reversible and selective *h*FAAH inhibitors with nanomolar potency. Here, we describe the synthesis of new β-lactam derivatives to evaluate the effect of imide conformational constraints on activity and to eliminate potential metabolic soft spots. Bicyclic derivatives were designed to lock the imide in a *syn* configuration, but showed reduced potency compared with non-cyclic analogs. Docking studies revealed that this weaker inhibition arises from an altered binding mode within the FAAH active site. In parallel, removal of ester and allyl groups did not affect inhibitory potency. Importantly, the optimized inhibitor enhanced *N*-acylethanolamine levels in J774 cells, supporting target engagement and suggesting improved metabolic stability. These results provide insights into the mode of action of β-lactam FAAH inhibitors and guide the development of more potent, stable derivatives.

1 | Introduction

Controlling endogenous levels of *N*-acylethanolamine has attracted significant interest due to its diverse and potent biological properties [1, 2]. This family of lipid mediators includes endocannabinoid lipids such as the *N*-arachidonoylethanolamine (anandamide, AEA, **1**) as well as non-endocannabinoid lipid mediators such as *N*-palmitoylethanolamine (PEA) and *N*-oleoylethanolamine (OEA) (Figure 1). Collectively, *N*-acylethanolamines (NAE) are endowed with numerous biological properties, such as regulating energy homeostasis as well as anti-inflammatory [3] and analgesic properties [4], to name a few.

Given the critical role played by the serine hydrolase fatty acid amide hydrolase (FAAH) in controlling the endogenous levels of NAE [5, 6], the last two decades have seen an intense development of FAAH inhibitors.

Over the years, various families of FAAH inhibitors have been developed, such as carbamates [3], boronic acids [7], and ureas [8] (Figure 1). Largely used FAAH inhibitors such as URB-597 [9] and PF-3845 [8] are characterized by their irreversible inhibition of FAAH through covalent bond formation, due to their electrophilic properties [10, 11].

Our laboratory has a keen interest in β-lactam derivatives, which led to the identification of β-lactam (**5**) as a potential hit (half-maximal inhibitory concentration [IC_{50}] = 4.5 μM) (Figure 2). Following extensive optimization involving a series of 30 compounds, a lead compound (**6**) was obtained, displaying an IC_{50}

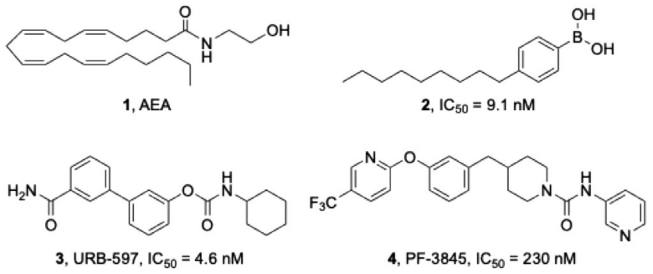

FIGURE 1 | Anandamide (**1**), boronic acid (**2**), URB-597 (**3**), PF-3845 (**4**).

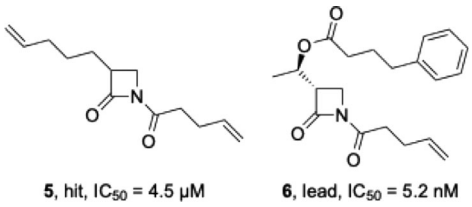

FIGURE 2 | β-Lactams demonstrating an inhibitory activity for *h*FAAH.

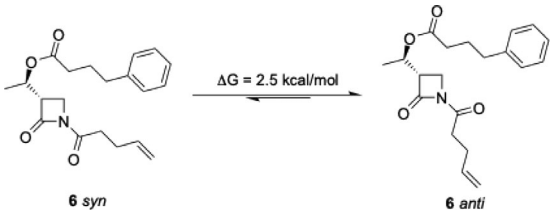

SCHEME 1 | Calculated equilibrium between *syn* and *anti* conformation of the lead compound **6**.

of 5.2 nM for *h*FAAH [12, 13]. Another interesting feature of these β-lactam inhibitors, and somewhat unexpected given the history of these compounds as irreversible serine hydrolase inhibitors, is the reversible nature of their FAAH inhibition [14, 15].

In the context of this research, we undertook a molecular modeling study (docking) to better understand the mechanisms of FAAH inhibition by β-lactams and their interactions with the active site of the enzyme. [13] Since the 3D structure of human FAAH has not yet been resolved by X-ray diffraction, we based our work on the humanized rat FAAH structure. [16] The models developed showed that the phenyl group of the lead fits into a pocket composed of three phenylalanine residues (Phe338, Phe381, Phe192), referred to as the "phenyl pocket." Additionally, the methyl group resides in a hydrophobic pocket within the enzyme's cavity, and the alkyl chain lies at the entrance of the ACB channel. Regarding the carbonyl functions of the imide, their conjugation with the lone pair of nitrogen (which is planar) forces them to be in the same plane. Two conformations are nevertheless possible: the two groups can be in *syn* or *anti*, with an equilibrium favoring the *anti* form by 2.5 kcal/mol (Scheme 1). [14] Docking data suggested, however, that the *syn* conformation is favored in the catalytic pocket as it allows for inhibitor-enzyme complex stabilization through hydrogen bonding between the two carbonyls and the serine and threonine residues of the catalytic triad.

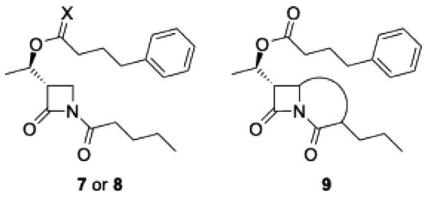

FIGURE 3 | Reduced version of the lead (X = O, **7**), ether, and reduced version of the lead (X = H,H, **8**), general scaffold of the bicyclic equivalents of the reduced lead (**9**).

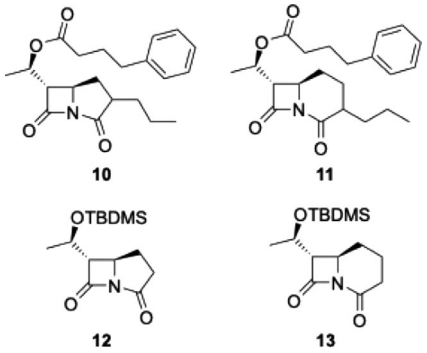

FIGURE 4 | [3.2.0] Bicyclic analog of the lead (**10**), [4.2.0] bicyclic analog of the lead (**11**), [3.2.0] bicyclic precursor (**12**), [4.2.0] bicyclic precursor (**13**).

We report here our study aiming at investigating further the mode of action of these β−lactam inhibitors by combining organic synthesis, biochemical investigations, and docking studies. In particular, we have synthesized and pharmacologically evaluated a series of bicyclic compounds (**11a,b** and **27**, Figure 4), enabling us to investigate the importance of the *syn*/*anti* conformation of the imide function as well as two reduced analogs of the lead, with a potential increased physiological stability (**7** and **8**, Figure 3).

2 | Results and Discussion

2.1 | Chemistry

2.1.1 | Bicyclic Compounds

When considering bicyclic β-lactams enabling to block of the two imide carbonyls in a *syn* configuration, several structures can be envisioned. Among these, we chose to focus on the [3.2.0] and [4.2.0] bicyclic skeletons, which led to the respective bicyclic analogs of our lead (**10** and **11**, Figure 4). To determine which bicycle would be the best candidate as an FAAH inhibitor, precursors **12** and **13** were prepared. These precursors differ from the target compounds by replacing the ester chain with a -OTBDMS protecting group and by the absence of the α−side chain of the imide carbonyl. Obtaining these two compounds and determining their IC_{50} will enable us to guide the next steps of our approach.

The precursor **12** was obtained in five steps from commercially available acetoxy-azetidinone **14** (Scheme 2). First, **14** undergoes substitution of the acetate by phenylsulfonate [17]. Next, an alkylation is carried out at C3 of the lactam using an in situ-generated

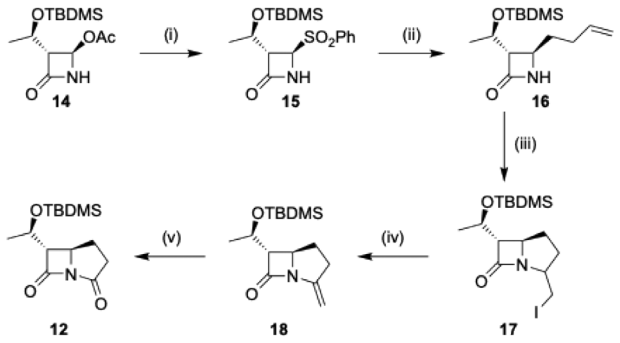

SCHEME 2 | (i) $PhSO_2Na$, dimethylformamide (DMF) 0°C to room temperature (RT), 4 h, 88%; (ii) but-3-en-1-ylmagnesium bromide, tetrahydrofuran (THF), 0°C to RT, 16 h, 51%; (iii) I_2, 2-methyloxirane, CH_2Cl_2, RT, 5 h, 55%; (iv) DBU, THF, RT, 24 h, 86% (crude); (v) ozone, CH_2Cl_2, SMe_2, 16 h, 69%.

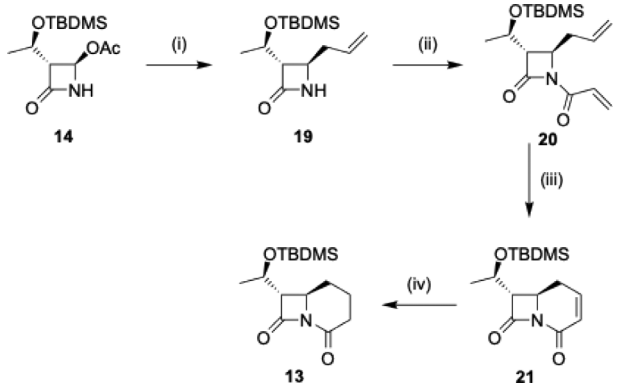

SCHEME 3 | (i) In, KI, allyl bromide, dimethylformamide (DMF), room temperature (RT), 4 h, 87%; (ii) (a) *n*BuLi, CH_2Cl_2, 0°C, 30 min, (b) acryloyl chloride, pyridine 0°C to 40°C, 77%; (iii) Grubbs II catalyst (5 mol%), CH_2Cl_2, RT, 16 h, 79%; (iv) H_2, Pd/C (10 mol%) AcOEt/EtOH (1:1), 16 h, 99%.

Grignard reagent, yielding compound **16**. Iodocyclization is then performed, leading to the formation of the second cycle of **17**. A β-elimination is subsequently executed, resulting in the formation of a carbon-carbon double bond (**18**). In the last step, the double bond is oxidized in the presence of ozone to generate the second carbonyl of the imide function and so obtain the [3.2.0] bicyclic precursor **12** with an overall yield of 11% over five steps.

The precursor **13** was obtained in four steps, also starting from the commercially available acetoxy-azetidinone **14**. First, the substitution of the acetate with an allyl group is carried out via the formation of an allylindium, resulting in the allylated compound **19** (Scheme 3). This latter is then *N*-acylated with acryloyl chloride, leading to compound **20** with two terminal double bonds that enable the formation of the second cycle of **21** through a ring-closing metathesis using a second-generation Grubbs catalyst. Once the bicycle **21** having an α,β-unsaturation is obtained, it is hydrogenated to yield the [4.2.0] bicyclic precursor **13** with an overall yield of 40% over four steps.

We then determined the potency of **12** and **13** against FAAH activity (see the Biochemistry section). Obtained IC_{50} values (288 and 92 nM for the **12** and **13**, respectively) suggest that bicyclic

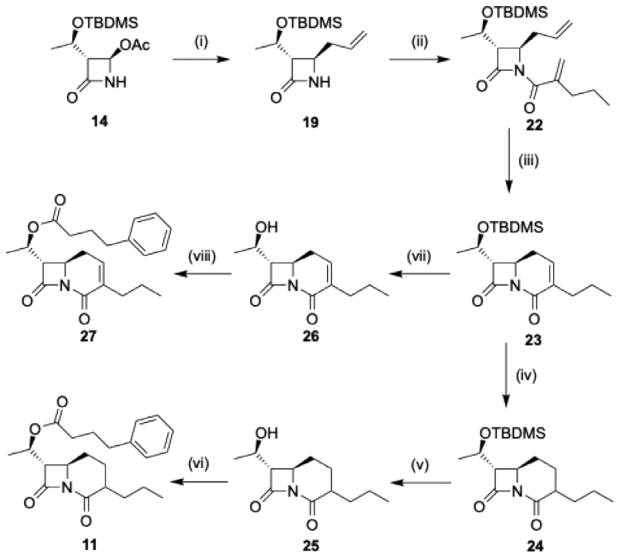

SCHEME 4 | (i) In, KI, allyl bromide, dimethylformamide (DMF), room temperature (RT), 4 h,87%; (ii) (a) *n*BuLi, CH_2Cl_2, 0°C, 30 min, (b) 2-methylenepentanoyl chloride, pyridine, 0°C to RT, 16 h, 67%; (iii) Grubbs II catalyst, CH_2Cl_2, 40°C, 24 h, 83%; (iv) H_2, Pd/C (10 mol%) AcOEt/EtOH (1:1), 16 h, 99%; (v) AcOH, H_2O, 90°C, 3 h, 91%; (vi) 4-phenylbutanoyl chloride, pyridine, CH_2Cl_2, RT, 24 h, 42% (dr = 55:45); (vii) AcOH, H_2O, 90°C, 3 h, quantitative, (viii) 4-phenylbutanoyl chloride, pyridine, CH_2Cl_2, RT, 24 h, 49%.

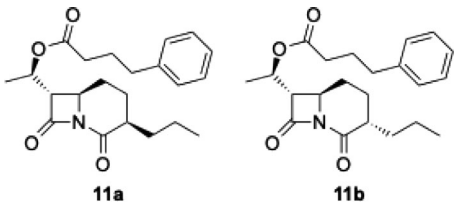

FIGURE 5 | The two diastereomers **11a** and **11b**.

β-lactams with a second 6-membered cycle are more effective in inhibiting FAAH than those with a [3.2.0] bicyclic core. These results led us to choose the next steps, the bicyclic analog of lead **11**, featuring a [4.2.0] bicyclic structure.

Our first idea was to synthesize the [4.2.0] bicycle **11** from intermediate **13**. However, the different approaches we tested did not enable us to introduce the desired α-alkyl chain (see Supporting Information). We therefore changed strategy and used an acyl chloride bearing the alkyl chain to obtain **22**, which, after ring-closing metathesis, provides bicyclic intermediate **23** (Scheme 4). This compound, with an α,β-unsaturation, was hydrogenated, resulting in **24**. Deprotection was subsequently carried out in the presence of acetic acid and water, yielding the corresponding alcohol **25**. Esterification with 4-phenylbutanoyl chloride led eventually to the [4.2.0] bicycle **11** with an overall yield of 19% over six steps.

Bicycle **11** was obtained as a mixture of two diastereomers, **11a** and **11b**, in a 55/45 ratio (Figure 5). These two diastereomers were separated by flash chromatography and identified by nuclear magnetic resonance (NMR) (see Supporting Information).

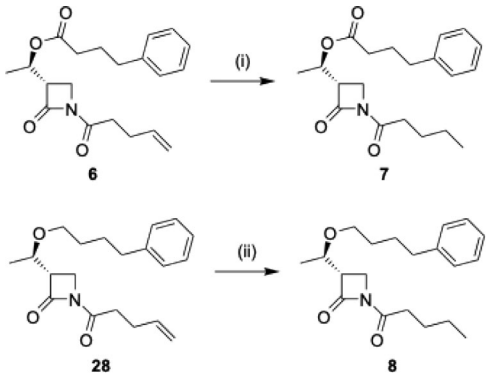

SCHEME 5 | (i) H_2, Pd/C (10 mol%) AcOEt/EtOH (1:1), 16 h, quantitative; (ii) H_2, Pd/C (10 mol%) AcOEt/EtOH (1:1), 16 h, quantitative.

TABLE 1 | Determination of the inhibition activity toward murine fatty acid amide hydrolase (FAAH).

Compound	IC_{50} [nM]	95% CI [nM][a]
URB-597[b]	20.0	12.4 to 32.1
6	4.9	3.8 to 6.4
8	10.2	7.9 to 13.1
11a	55.0	42.1 to 72.2
11b	197	157 to 247
27	171	122 to 240

[a]The data are represented by the mean ± SD ($n = 3$). [b]URB-597 was used as a reference.

An analog of bicycle **11** was also successfully obtained (**27**). It differs from the latter by maintaining the α,β-unsaturation. To achieve this, compound **23** was directly deprotected in the presence of acetic acid and water before esterification with 4-phenylbutanoyl chloride to obtain bicycle **27** with an overall yield of 21% over five steps (see Scheme 4).

2.1.2 | Reduced Derivatives

Concerned about the stability of these inhibitors in a physiological environment, we decided to investigate the influence of the double bond at the end of the α-alkyl chain, which is absent in the synthesized [4.2.0] bicyclic derivatives (**11** and **27**), as well as of the ester function on FAAH inhibition. Accordingly, we prepared compounds **7** and **8** by hydrogenation of **6** [14] and **28** [12] (Scheme 5).

3 | Biochemical and Pharmacological Assessment of the Inhibitors

We assessed the ability of the different compounds to inhibit the hydrolysis of AEA. In our assay conditions, using mouse brain homogenates, we obtained an IC_{50} value of 4.9 nM for **6**, a value similar to the one we previously reported using recombinant *h*FAAH (Table 1) [14]. Interestingly, our lead compound is in the same range of activity as CAY-10402, a commercial and reference FAAH α-ketoheterocycle reversible inhibitor. [18]

As mentioned, for bicycle **11**, two diastereomers are possible, namely **11a** and **11b**, differing by the absolute configuration of the carbon in α to the carbonyl on the six-membered ring. For the (*R*) derivative (**11a**), we obtained an IC_{50} value of 55 nM, compared to a value of 197 nM for the (*S*) isomer (**11b**). Interestingly α,β-unsaturated equivalent of bicycle **11**, i.e., **27**, showed an inhibitory potency (IC_{50} = 171 nM) similar to that of **11b**, emphasizing the importance of the stereogenic center α configuration to the carbonyl.

Taken together, the three bicycles **11a**, **11b**, and **27** have a significantly lower potency as compared to the lead compound (**6**). Based on our working hypothesis, this is unexpected since the bicyclic structure forces the two carbonyls into a *syn* configuration, presumably leading to an enhanced anchor of the ligand within the enzyme's active site, unlike the *anti* configuration [14].

In addition to our work on the core part of the lead, we wanted to assess whether two moieties that could potentially decrease the activity of the lead (**6**) in a biological context (namely, the α-alkyl chain double bond and the ester moiety) were dispensable. Specifically, we replaced the allyl moiety of **6** by its saturated analog (**7**) and found that this does not significantly affect the potency of the compound (IC_{50} = 4.9 and 8.0 nM for **6** and **7**, respectively). Similarly, replacing the ester moiety of **7** by its ether analog did not affect the activity (IC_{50} = 10.2 nM for **8**). Thus, overall, when comparing the potency of **8** to the potency of the lead (**6**), only a modest reduction in the in vitro activity is noticed.

To further support the interest of this series of FAAH inhibitors, we assessed their ability to increase NAE levels in intact cells, such as J774 cells. This cellular system has previously demonstrated the presence of FAAH activity and an increase in NAE levels using the reference inhibitor PF-3845 [19].

As expected, following the incubation of J774 cells with a reference FAAH inhibitor (PF-3845), we found a strong increase in PEA, SEA, OEA, and AEA cellular levels (Figure 6). Our lead compound (**6**) increased the levels of AEA, but not the levels of PEA, SEA, and OEA. The bicycle **11a** had a similar effect on the NAE levels, whereas its ether analog **8** had the strongest effect on NAE levels among the four β-lactams assessed. Interestingly, although sharing a similar potency in the biochemical assay, **8** was much more efficient in increasing NAE levels when compared to its ester analog (**7**). One explanation could be a potentially greater stability of **8** in biological conditions.

4 | Docking Studies

Our previous docking studies were carried out on a model of human FAAH, based on the crystallographic structure of humanized rat FAAH. [13, 14, 16] Two main binding modes were discussed for **6**. One of them (mode 1) directs the *syn* conformation of the imide moiety toward the catalytic triad (Ser217, Ser241, and Lys142) and the phenyl chain in the so-called "phenyl pocket" composed of three phenylalanine residues (Phe388, Phe381, and Phe192). In the second mode (mode 2), the

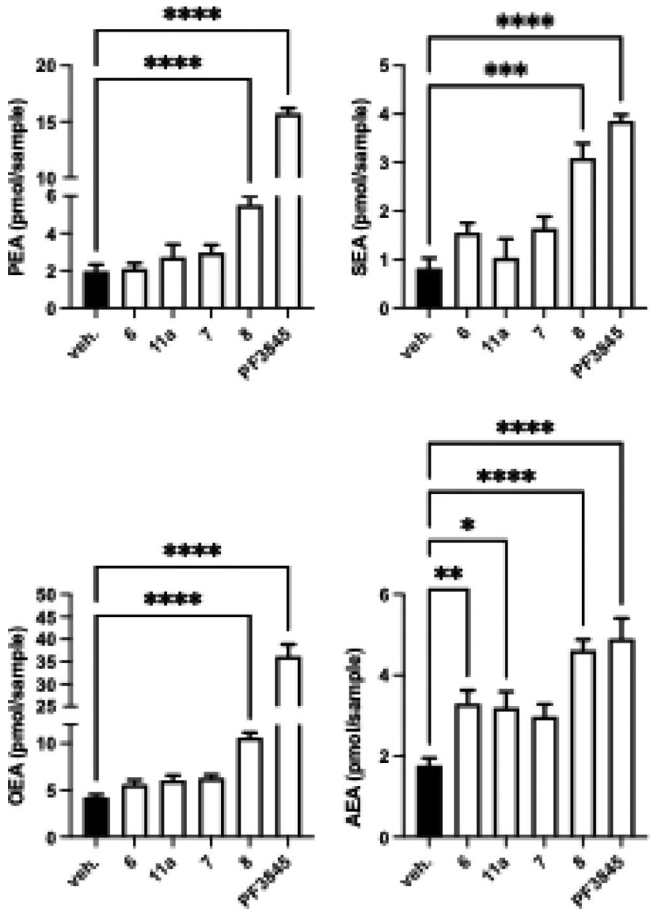

FIGURE 6 | *N*-acylethanolamines (NAE) levels were measured by liquid chromatography-tandem mass spectrometry (LC-MS/MS) following incubation of J774 cells in the presence of 10 μM of each inhibitor or vehicle (dimethyl sulfoxide [DMSO] 0.1%, veh) for 5 h.

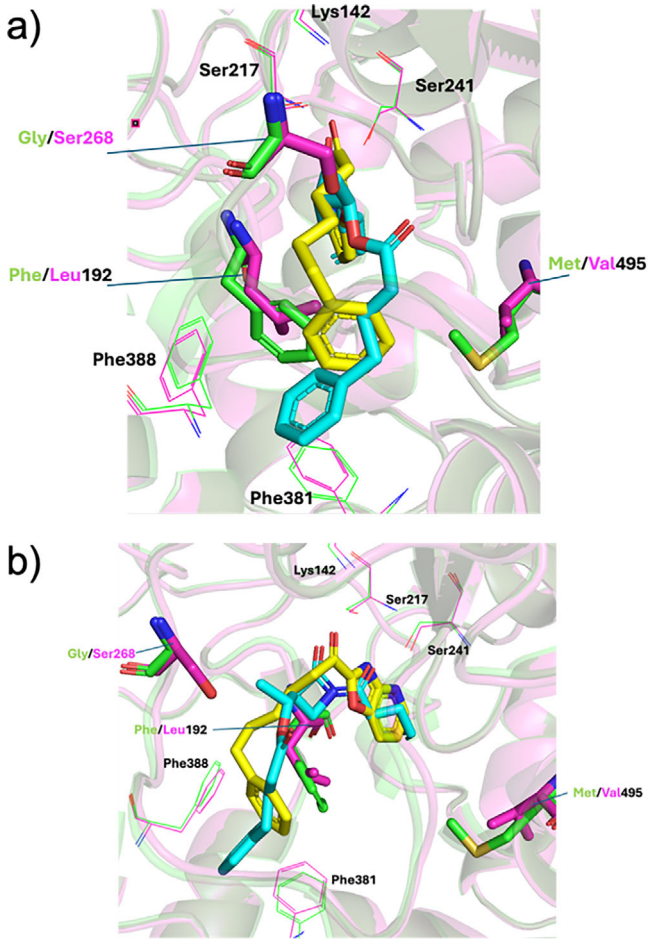

FIGURE 7 | Docking of the active site of the human (green) and mouse (magenta) fatty acid amide hydrolase (FAAH) with **6** (turquoise) and CAY-10402 (yellow) in the binding mode 1, in two views, (a) and (b).

ester group interacts with the catalytic triad, while the allyl chain is in the phenyl pocket.

As most preclinical models in which FAAH inhibitors are tested are mouse models, we reasoned that using a mouse FAAH model (pdb code: 2VYA) would be an appropriate approach for our SAR explorations. The two enzymes exhibit a high degree of sequence identity (84%), and within the binding site, only three amino acid residues are different: i) the Phe 192 of the Phenyl pocket is a leucine in the mouse enzyme, ii) the Gly 268, a serine, and iii) the Met 495, a valine (Figure 7a,b). These differences do not appear to affect ligand binding, since the two binding modes could be recovered for **6** inside the mouse FAAH, with a preference for the first binding mode. Based on these observations, we used mouse FAAH for our next studies.

The preference of **6** for mode 1 is supported by the fact that inhibition tests show that its allyl chain is not essential (see **6** vs **7**). Indeed, the latter has no specific interaction in the active site, while in mode 2 it could interact by π-π interactions in the phenyl pocket. Remarkably, docking of CAY-10402 also positions the reference inhibitor in mode 1: i) with the phenyl group in the phenyl pocket and ii) the carbonyl and nitrogen of the oxazole in the same place as the imide moiety of **6**.

As shown, the three bicyclic compounds we synthesized (**11a**, **11b**, **27**) are weaker FAAH inhibitors than **6** and **7**. Our docking results suggest that this observation may arise from the fact that these three compounds are restricted to bind in mode 2, unlike **6**, due to structural constraints. Indeed, their alkyl chain is in the phenyl pocket while their phenyl group lies at the entrance of the ACB channel (Figure 8a,b). Several possibilities for interaction with the enzyme are therefore lost as compared to mode 1 (Table 2). First, only one carbonyl moiety ("CO_{ester}", from the ester group) is involved in H-bonding with the two catalytic serines (Ser241 and Ser217). Indeed, in the binding mode 1, **7** could form 3 H-bonds via its imide moiety (CO_{lactam} and CO_{exo}). Secondly, the imide group is not involved in any interaction, and the H-bond observed between Ser268 and the CO_{ester} in **7** is lost. For **11b** and **27**, they are positioned in the same way as **11a**, apart from the alkyl chain, which is differently positioned (Figure 9): in the case of **11b** and **27**, the chain is closer to Leu380, which could lead to a steric clash, and potentially explains their slightly higher IC_{50}.

In order to further support mode 1 for our lead compounds **6** and **7**, as well as to guide the next syntheses, the compound **8**, i.e., **7** lacking the CO_{ester} group, was docked in the FAAH active site. It was also found in mode 1 with a slightly weaker score function than **7**, probably due to the loss of the weak H-bond with Ser268.

TABLE 2 | Non-covalent interactions between mFAAH and the compounds **6**, **7**, **11a**, and **8**.

Entry	Compound	Non-covalent interactions[a] [Å]	Binding score function	IC_{50} [nM][b]
1	**6**	***Mode 1*** $Ser_{217}(O)\ldots O(CO_{lactam})$: 3.4 $Ser_{217}(O)\ldots O(CO_{exo})$: 2.8 $Ser_{241}(O)\ldots O(CO_{exo})$: 2.1 $Ser_{268}\ldots O(CO_{ester})$: 3.8 $Phe_{381}\ldots$ Phe: 4.4 $Val_{270}(CH)\ldots$ Phe: 3.3	63.7	4.9
2	**7**	***Mode 1*** $Ser_{217}(O)\ldots O(CO_{lactam})$: 3.8 $Ser_{217}(O)\ldots O(CO_{exo})$: 2.7 $Ser_{241}(O)\ldots O(CO_{exo})$: 2.4 $Ser_{268}\ldots O(CO_{ester})$: 2.2 $Phe_{381}\ldots$ Phe: 4.8 $Val_{270}(CH)\ldots$ Phe: 3.0	66.5	8.0
3	**11a**	***Mode 2*** $Ser_{217}(O)\ldots O(CO_{ester})$: 2.6 $Ser_{241}(O)\ldots O(CO_{ester})$: 2.7 $Phe_{381}\ldots$ CH: 3.6 $Leu_{192}(CH)\ldots$ Phe: 2.9	52.10	55.0
4	**8**	***Mode 1*** $Ser_{217}(O)\ldots O(CO_{lactam})$: 3.6 $Ser_{217}(O)\ldots O(CO_{exo})$: 2.7 $Ser_{241}(O)\ldots O(CO_{exo})$: 2.4 $Phe_{381}\ldots$ Phe: 4.8 $Val_{270}(CH)\ldots$ Phe: 3.0	62.40	10.2

[a]Non-covalent interactions are given for H-bonds (in blue), π-π interactions (measured as the distance between aromatic centroids, in purple), and CH-π interactions (measured as the distance between the H atom and the aromatic centroid, in green).
[b]The data are represented by the mean ± SD (n = 3).

5 | Conclusion

We have synthesized and pharmacologically evaluated seven new β-lactam derivatives in order to investigate further the mode of action of β-lactamic inhibitors of FAAH. In particular, bicyclic derivatives **11a**, **11b**, and **27** were developed to assess the importance of the imide conformational equilibrium, while **7** and **8**, lacking one or two of the reactive functional groups, were designed to increase the biological stability of these β-lactam inhibitors.

Unexpectedly, the bicyclic compounds featuring an imide group blocked in *syn* configuration show a lower potency compared to their non-cyclic analog, the lead compound **6**, as revealed by their respective IC_{50}. Docking studies indicate that this weaker FAAH inhibition can be explained by a change in the binding mode. Indeed, in the case of bicyclic structures (**11a-b** and **27**), a second binding mode (mode 2) is operative in which it is the ester group that interacts with the catalytic triad, and not the imide function, while the alkyl chain is in the phenyl pocket.

The reduced forms of our lead, lacking the double bond (**7**) as well as the ester group (**8**), did not show any significantly different FAAH inhibition activity. However, we in cellulo assays revealed that **8** has the strongest effect on NAE levels in J774 cells among all the tested β-lactams, possibly due to the enhanced physiological stability.

Overall, our combined synthetic, biochemical, pharmacological, and computational study provides a better understanding of the mode of action of β-lactam FAAH inhibitors and allows identifying new derivatives with increased activity in cellulo.

6 | Experimental

6.1 | Chemistry

(3*S*,4*R*)-4-Allyl-3-((*R*)-1-((*tert*-butyldimethylsilyl)oxy)ethyl) azetidin-2-one (19). In a dried three-neck round-bottom flask under inert conditions, KI (3.1 g, 18.7 mmol, 3.0 eq.) and indium (1.435 g, 12.5 mmol, 2.0 eq.) were added to 50 mL of dimethylformamide (DMF), followed by allyl bromide (1.618 mL, 18.7 mmol, 3.0 eq.). After 1 h, the commercially available azetidinone **14** (1.782 g, 6.2 mmol, 1.0 eq.) was introduced into the solution. The mixture was stirred for 4 h, then diluted with diethyl ether. The organic phase was washed with a saturated NH_4Cl solution, then with brine, and concentrated under reduced pressure. A white powder was obtained. Yield: 98% ^{1}H NMR (300 MHz, $CDCl_3$) δ (ppm): 5.88 (bs, 1H), 5.84–5.65 (m, 1H), 5.21–5.05 (m, 2H), 4,16 (qd, J = 6.3; 4.9 Hz), 3.69 (ddd, J = 7.7,

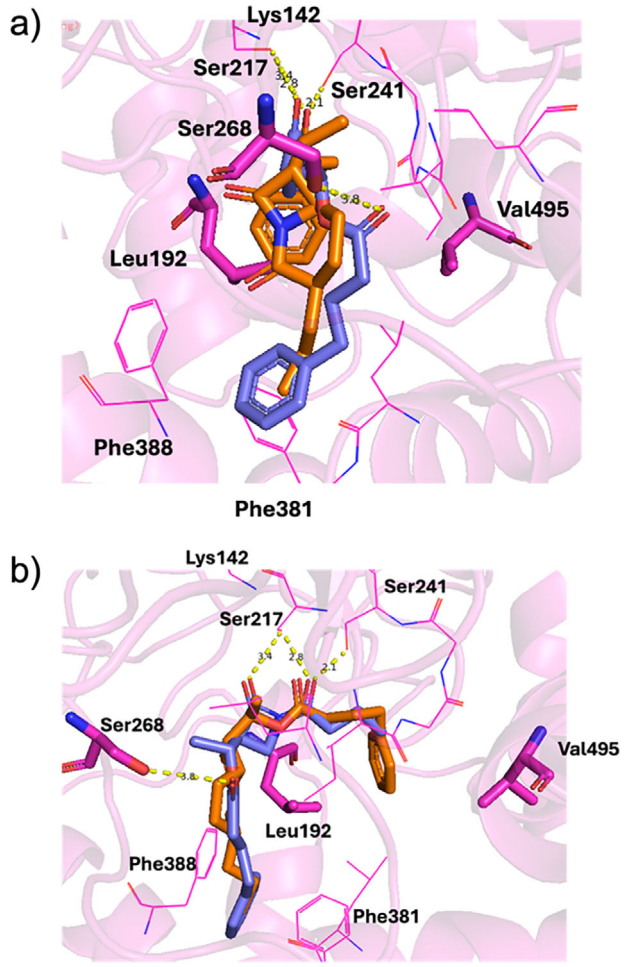

FIGURE 8 | Docking of the active site of the mouse fatty acid amide hydrolase (FAAH) (magenta) with **7** (purple) and **11a** (orange), in two views, (a) and (b).

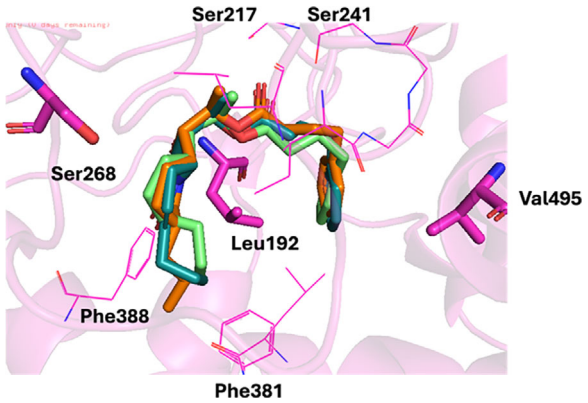

FIGURE 9 | Docking of the active site of the mouse (magenta) fatty acid amide hydrolase (FAAH) with **11a** (orange), **11b** (light green), and **27** (turquoise).

7.0, 5.0 Hz, 1H), 2.77 (ddd, J = 5.0, 2.2, 0.9 Hz, 1H), 2.48–2.24 (m, 2H), 1.20 (d, J = 6.2 Hz, 3H), 0.87 (s, 9H), 0.06 (s, 3H), 0.06 (s, 3H). ^{13}C NMR (75 MHz, $CDCl_3$) δ (ppm): 168.6, 133.9, 118,2, 65.6, 63.9, 50.3, 39.6, 25,9, 22.9, 18.1, -4.1, -4.8. High-resolution mass spectrometry (HRMS) (APCI): m/z found = 270.18838; calcd. for $[M+H]^+$: 270.18819. Fourier-transform infrared (FT-IR) (cm^{-1}): 3082, 2928, 2856, 1751, 1250, 1136, 1053, 968, 828, 776, 722. Melting point (m.p.): 83°C.

(3*S*,4*R*)-4-(But-3-en-1-yl)-3-((*R*)-1-((*tert*-butyldimethylsilyl)oxy)ethyl)azetidin-2-one (22). In a dried three-neck round-bottom flask under inert conditions, oxalyl chloride (0.283 mL, 3.3 mmol, 3.0 eq.) was added to a solution of 2-methylenepentanoic acid (377 mg, 3.3 mmol, 3.0 eq.) in 15 mL of dichloromethane (DCM). One drop of DMF was then added. The mixture was stirred at room temperature for 2 h until the off-gassing ceased. Meanwhile, in another three-neck round-bottom flask under inert conditions, **19** (269 mg, 1.1 mmol, 1.0 eq.) was dissolved in 15 mL of DCM. *n*BuLi (1.3 mmol, 1.3 eq.) was added dropwise at 0°C to the **19** solution, and the resulting mixture was stirred at 0°C for 30 min. The first reaction solution containing 2-methylenepentanoic chloride was then added dropwise at 0°C *via* cannulation between the three-neck round-bottom flasks. The mixture was stirred at 40°C for 24 h. The solution was washed with a saturated NH_4Cl solution, followed by brine, and dried over $MgSO_4$. The product was concentrated under reduced pressure. The crude product was purified by flash chromatography on silica gel using hexane/AcOEt (95/5), and a colorless oil was obtained. Yield: 51%.^{1}H NMR (300 MHz, $CDCl_3$) δ (ppm): 5.91 (s, 1H), 5.84–5.69 (m, 1H), 5.67 (s, 1H), 5.19–5.14 (m, 1H), 5.12 (d, J = 1.2 Hz, 1H), 4.27 (m, 2H), 2.88 (t, J = 3.4 Hz, 1H), 2.82–2.66 (m, 1H), 2.56–2.04 (m, 3H), 1.55–1.40 (m, 2H), 1.16 (d, J = 6.3 Hz, 3H), 0.92 (t, J = 7.4 Hz, 3H), 0.81 (s, 9H), 0.04 (s,3H), 0.00 (s, 3H). ^{13}C NMR (75 MHz, $CDCl_3$) δ (ppm): 167.5, 165.3, 143.0, 132.6, 124.2, 119.3, 65.0, 60.4, 51.2, 36.4, 34.4, 25.8, 22.6, 21.3, 17.9, 13.8, -4.1, -5.0. HRMS (electrospray ionization [ESI]): m/z found = 366.24591; calcd. for $[M+H]^+$: 366.24590.

(6*R*,7*S*)-7-((*R*)-1-((*Tert*-butyldimethylsilyl)oxy)ethyl)-3-propyl-1-azabicyclo[4.2.0]oct-3-ene-2,8-dione (23). In a dried round-bottom flask under inert conditions, Grubbs II catalyst (25 mg, 0.03 mmol, 0.05 eq.) was added, followed by a solution of **22** (219 mg, 0.6 mmol, 1.0 eq.) in 2.5 mL of DCM. The mixture was stirred at 40°C for 16 h. The product was concentrated under reduced pressure, and the crude product was purified by flash chromatography on silica gel using hexane/AcOEt (80/20). A white powder was obtained. Yield: 83%.^{1}H NMR (300 MHz, $CDCl_3$) δ (ppm): 6.41–6.38 (m, 1H), 4.28–4.22 (m, 1H), 4.19–4.12 (m, 1H), 3.07 (dd, J = 4.9, 3.0 Hz, 1H), 2.67–2.58 (m, 1H), 2.51–2.45 (m, 1H), 2.42–2.30 (m, 1H), 2.20–2.10 (m, 1H), 1.51–1.43 (m, 2H), 1.22 (d, J = 6.2 Hz, 3H), 0.91 (t, J = 7.3, 3H), 0.86 (s, 9H), 0.08 (2s, 6H). ^{13}C NMR (75 MHz, $CDCl_3$) δ (ppm): 159.3, 136.1, 110.1, 66.9, 65.2, 50.2, 28.9, 25.8, 22.6, 21.7, 18.0, 13.8, -4.1, -4.9. HRMS (APCI): m/z found = 338.21460; calcd. for $[M+H]^+$:338.21460. FT-IR (cm^{-1}): 2956, 2928, 2853, 1798, 1681, 1291, 834, 777. m.p.: 84°C.

(6*R*,7*S*)-7-((*R*)-1-((*Tert*-butyldimethylsilyl)oxy)ethyl)-3-propyl-1-azabicyclo[4.2.0]octane-2,8-dione (24). In a dried round-bottom flask under inert conditions, Pd/C 10% (0.3 mmol, 1.0 eq.) was added, followed by a solution of **23** (101 mg, 0.3 mmol, 1.0 eq.) in 10 mL of EtOH and 10 mL of AcOEt. The mixture was stirred at room temperature for 16 h under a hydrogen atmosphere. The solution was filtered through a pad of celite and concentrated under reduced pressure. A white powder was obtained. Yield: 99%. ^{1}H NMR (500 MHz, $CDCl_3$) δ (ppm): 4.28–4.22 (m, 1H), 4.06–3.95 (m, 1H), 3.12 (dd, J = 4.3, 3.6 Hz, 1H

(dia 1)), 3.00 (dd, J = 4.5, 3.2 Hz, 1H (dia 2)), 2.40–2.30 (m, 1H (dia 1)), 2.25–2.20 (m, 1H (dia 2)), 2.18–2.05 (m, 2H), 1.91–1.77 (m, 1H), 1.76–1.66 (m, 1H), 1.64–1.48 (m, 2H), 1.45–1.23 (m, 2H), 1.19 (d, J = 6.3 Hz, 3H), 0.94–0.88 (m, 3H), 0.86 (s, 9H), 0.06 (s, 6H). ^{13}C NMR (125 MHz, $CDCl_3$) δ (ppm): 170.2 (dia 1), 169.5 (dia 2), 165.8 (dia 1), 165.4 (dia 2), 67.4 (dia 1), 67.3 (dia 2), 65.0 (dia 1), 64.9 (dia 2), 54.1 (dia 1), 52.5 (dia 2), 41.9 (dia 1), 39.9 (dia 2), 34.6 (dia 1), 32.5 (dia 2), 28.0 (dia 1), 27.1 (dia 2), 26.1 (dia 1), 26.0 (dia 2), 22.7, 22.6, 20.5 (dia 1), 19.9 (dia 2), 18.0, 14.2, -4.6, -4.9. HRMS (ESI): m/z found = 362.21085; calcd. for $[M+Na]^+$: 362.21204.

(6*R*,7*S*)-7-((*R*)-1-Hydroxyethyl)-3-propyl-1-azabicyclo[4.2.0]octane-2,8-dione (25). In a round-bottom flask, **24** (68 mg, 0.2 mmol, 1.0 eq.) was added to 1.4 mL of AcOH and 0.5 mL of H_2O. The solution was heated to 90°C and stirred for 3 h. The product was then concentrated under reduced pressure. The crude product (a yellow oil) was directly used in the next step. ^{1}H NMR (500 MHz, $CDCl_3$) δ (ppm) (only the characteristic peaks are reported here): 3.20 (dd, J = 5.3, 3.6 Hz, 1H (dia 1)), 3.07 (dd, j = 5.3, 3.2 Hz, 1H (dia 2)), 1.20 (d, J = 6.4, 3H). ^{13}C NMR (125 MHz, $CDCl_3$) δ (ppm): 170.4 (dia 1), 169.6 (dia 2), 165.6 (dia 1), 165.2 (dia 2), 66.8, 64.7, 53.6 (dia 1), 52.8 (dia 2), 42.0, 39.9, 32.5, 29.8, 28.0, 27.1, 26.1, 21.8, 20.5, 20.0, 14.0. HRMS (APCI): m/z found = 226.14366; calcd. for $[M+H]^+$: 226.14377. FT-IR (cm^{-1}): 3327, 2958, 2928, 2872, 1802, 1697, 1638, 1301.

(*R*)-1-((3*R*,6*R*,7*S*)-2,8-Dioxo-3-propyl-1-azabicyclo[4.2.0]octan-7-yl)ethyl 4-phenylbutanoate (11a) *and* (*R*)-1-((3*S*,6*R*,7*S*)-2,8-dioxo-3-propyl-1-azabicyclo[4.2.0]octan-7-yl)ethyl 4-phenylbutanoate (11b). In a dried three-neck round-bottom flask under inert conditions, 4-phenylbutanoyl chloride (256 mg, 1.4 mmol, 1.6 eq.) and pyridine (0.161 mL, 2.0 mmol, 2.3 eq.) were added to a solution of **25** (203 mg, 0.9 mmol, 1.0 eq.) in 20 mL of DCM. The mixture was stirred at room temperature for 24 h. The solution was washed with a saturated $NaHCO_3$ solution, followed by 1 M HCl, then with brine, and dried over $MgSO_4$. The product was concentrated under reduced pressure. The crude product was purified by flash chromatography on silica gel using cyclohexane/AcOEt (80/20). The two diastereomers were successfully separated completely, and yellow oil was obtained for both products. **Diastereomer 1 (3*R*, 11a)** ^{1}H NMR (500 MHz, $CDCl_3$) δ (ppm): 7.29 (t, J = 7.5 Hz, 2H), 7.22–7.15 (m, 3H), 5.26 (quint, J = 6.4 Hz, 1H), 3.98–3.92 (m, 1H), 3.16 (dd, J = 6.6, 3.3 Hz, 1H), 2.64 (dd, J = 8.6, 6.7 Hz, 2H), 2.31 (t, J = 7.5 Hz, 2H), 2.27–2.20 (m, 1H), 2.19–2.04 (m, 2H), 1.98–1.89 (m, 2H), 1.88–1.78 (m, 1H), 1.76–1.67 (m, 1H), 1.65–1.55 (m, 2H), 1.46–1.31 (m, 5H), 0.92 (t, J = 7.4 Hz, 3H). ^{13}C NMR (125 MHz, $CDCl_3$) δ (ppm): 172.6, 170.1, 163.3, 141.3, 128.3, 128.2, 126.2, 67.3, 64.5, 54.0, 39.9, 35.1, 33.7, 32.5, 26.5, 26.1, 25.9, 20.5, 18.6, 14.1. HRMS (ESI): m/z *found* = 372.21688; calcd. for $[M+H]^+$: 372.21693. FT-IR (cm^{-1}): 2957, 2936, 2872, 1804, 1733, 1700, 1298, 1135. **Diastereomer 2 (3*S*, 11b)** ^{1}H NMR (500 MHz, $CDCl_3$) δ (ppm): 7.29 (t, J = 7.7 Hz, 2H), 7.21–7.15 (m, 3H), 5.26 (quint, J = 6.4 Hz, 1H), 3.92 (dt, J = 11.1, 3.7 Hz, 1H), 3.30 (dd, J = 6.5, 3.7 Hz, 1H), 2.70–2.61 (m, 2H), 2.39-2.33 (m, 1H), 2.33–2.28 (m, 2H), 2.20–2.08 (m, 2H), 1.99–1.90 (m, 2H), 1.88–1.79 (m, 1H), 1.56–1.47 (m, 3H), 1.46–1.31 (m, 5H), 0.92 (t, J = 7.3 Hz, 3H). ^{13}C NMR (125 MHz, $CDCl_3$) δ (ppm): 172.6, 169.4, 163.7, 141.3, 128.6, 128.5, 126.2, 67.2, 64.4, 55.8, 42.0, 35.1, 34.3, 33.7, 28.0, 26.9, 26.5, 19.9, 18.5, 14.0. HRMS (ESI): m/z found = 372.21685; calcd. for $[M+H]^+$: 372.21693. FT-IR (cm^{-1}): 2957, 2931, 1804, 1735, 1687, 1298, 1137.

(*R*)-1-((*S*)-2-Oxo-1-pentanoylazetidin-3-yl)ethyl 4-phenylbutanoate (7). In a dried round-bottom flask under inert conditions, Pd/C 10% (0.09 mmol, 1.0 eq.) was added, followed by a solution of **6** (32 mg, 0.09 mmol, 1.0 eq.), previously obtained by Feledziak et al., in 10 mL of EtOH and 10 mL of AcOEt. The mixture was stirred at room temperature for 16 h under a hydrogen atmosphere. The solution was filtered through a pad of celite and concentrated under reduced pressure. A yellow oil was obtained. Yield: quantitative. ^{1}H NMR (300 MHz, $CDCl_3$) δ (ppm): 7.31–7.26 (m, 2H), 7.22–7.13 (m, 3H), 5.28 (quint, J = 6.3 Hz, 1H), 3.68–3.63 (m, 1H), 3.54–3.50 (m, 1H), 3.41–3.36 (m, 1H), 2.70–2.56 (m, 4H), 2.29 (t, J = 7.5 Hz, 2H), 1.92 (quint, J = 7.8 Hz, 2H), 1.61 (quint, J = 8.4 Hz, 2H), 1.44–1.29 (m, 5H), 0.91 (t, J = 7.3 Hz, 3H). ^{13}C NMR (75 MHz, $CDCl_3$) δ (ppm): 172.5, 171.4, 164.5, 141.2, 128.6, 128.5, 126.2, 67.4, 53.6, 40.0, 36.4, 35.2, 33.8, 26.6, 26.3, 22.4, 18.5, 13.9. HRMS (APCI): m/z found = 346.20115; calcd. for $[M+H]^+$: 346.20128.

(*S*)-1-Pentanoyl-3-((*R*)-1-(4-phenylbutoxy)ethyl)azetidin-2-one (8). In a dried round-bottom flask under inert conditions, Pd/C 10% (0.03 mmol, 1.0 eq.) was added, followed by a solution of **28** (10 mg, 0.03 mmol, 1.0 eq.), previously obtained by Feledziak et al., in 1 mL of EtOH and 1 mL of AcOEt. The mixture was stirred at room temperature for 16 h under a hydrogen atmosphere. The solution was filtered through a pad of celite and concentrated under reduced pressure. A yellow oil was obtained. Yield: quantitative. ^{1}H NMR (300 MHz, $CDCl_3$) δ (ppm): 7.35–7.05 (m, 5H), 3.88–3.74 (m, 1H), 3.66–3.52 (m, 2H), 3.43–3.28 (m, 2H), 3.27–3.20 (m, 1H), 2.93–2.52 (m, 4H), 1.70–1.51 (m, 4H), 1.45–1.14 (m, 7H), 0.90 (t, J = 7.4 Hz, 3H). ^{13}C NMR (75 MHz, $CDCl_3$) δ (ppm): 171.3, 166.3, 142.4, 128.5, 125,9, 72.0, 69.1, 55.0, 39.6, 16.4, 35.8, 29.9, 28.2, 26.4, 22.4, 18.1, 13.9.

7 | Biochemical and Pharmacological Assessment of the Inhibitors

7.1 | Determination of IC_{50} Values

Studies involving mouse tissue were conducted in accordance with the EU Directive 2010/63/EU, transformed into the Belgian Law of May 29, 2013, regarding the protection of laboratory animals (lab agreement number LA1230365) and were approved by the animal studies ethics committee of the health sector of the UCLouvain (07-OTLADDB-2023-7). Mice (from Janvier Labs) were housed in filter-top cages under controlled conditions of temperature (20–22°C) and artificial light (12-h light-dark cycle), and supplied with drinking water and food ad libitum. Mice were euthanized following the guidelines in place, and the brain rapidly recovered and was snap frozen in liquid nitrogen. Mouse brain homogenates were obtained by homogenising C57BL/6 mice brains (4°C, PBS, pH 7.4) and then centrifuging the resulting homogenate at 15 000 g for 20 min. The pellet was recovered, resuspended in PBS, and centrifuged again (15 000 g, 20 min). The pellet obtained was finally resuspended in PBS, the protein content determined, and the resulting membrane preparation stored at -80°C until use.

For the biochemical assay, the substrate (2 μM AEA and 50 000 dpm ofl'[^{3}H]-AEA) was incubated, in a total volume of 200 μL (10 mM Tris-HCl, 1 mM EDTA, 0.1% (w/v) BSA, pH 7.4), in the presence of mouse brain membranes and the compounds of interest (or vehicle (DMSO, 5%) during 10 min at 37°C. The enzymatic reaction was stopped by placing the tubes on ice and adding 400 μL of ice-cold chloroform—methanol (1:1, v/v). Following vigorous mixing, the tubes were centrifuged (850 g, 5 min) to favor phase separation. The supernatant (200 μL) was recovered and the radioactivity assessed by liquid scintillation counting. In all assays, tubes containing buffer, vehicle and the substrate were similarly processed to account for any non-enzymatic hydrolysis. This value was systematically subtracted from the other results.

7.2 | Cell Studies

The general procedure for the study of inhibitors in J774 macrophage cells is described below [19].

7.2.1 | Cell Culture

The murine macrophage cell line J774 (RRID:CVCL_4692) (a kind gift from Prof. M.-P. Mingeot, LDRI, UCLouvain) was routinely cultured under standard conditions (37°C in a humidified 5% CO_2 incubator) in RPMI 1640 medium containing 10% fetal bovine serum (FBS) and antibiotics (100 units/mL of penicillin and 100 μg/mL of streptomycin).

7.2.2 | NAE Quantification by Ultra-Performance LC-Tandem MS

Cells (10^7 cells/condition) were seeded in 10% FBS media for 16 h prior to the experiment. Then cells were incubated in media containing 1% FBS and the molecules of interest (10 μM) or vehicle (DMSO, 0.1%). At the end of the incubation, the media were removed and the cells recovered using PBS (2 mL) followed by methanol (MeOH, 4 mL), and transferred to DCM (CH_2Cl_2, 8 mL) containing the internal standards (d_4-PEA; d_4-AEA; d_4-OEA; d_4-SEA). Following vigorous mixing and sonication, the samples were centrifuged, and the organic layer was recovered and then dried under a stream of N_2. The resulting lipid fraction was pre-purified by solid-phase extraction over silica. Following a first step with hexane—*i*POH (99:1), the lipids of interest were eluted using hexane—*i*POH (7:3). The resulting lipid fractions were analysed according to the protocol used in previous studies, by using an ultra-performance LC (UPLC) system coupled to a Xevo-TQ-S Mass Spectrometer (Waters Corporation, Milford, Massachusetts, USA) [1]. An Acquity UPLC BEH C18 column (1.7 mm, 2.1 × 50 mm; Waters Corporation) connected to an in-line filter unit and maintained at 40°C was used for analyte separation in conjunction with a 0.2 mL/min gradient. Mobile phases A and B were composed of methanol-water-acetic acid (75:24.9:0.1, v/v/v) and methanol-acetic acid (99.9:0.1, v/v), respectively. An electrospray ionisation source in positive mode was used. The software MassLynx was used for data acquisition and processing. For each NAE of interest, the ratio between the area under the curve (AUC) of the peak and the AUC of the peak of the corresponding internal standard was determined. Calibration curves were obtained using similar conditions, and the amounts of NAE in the samples were calculated by linear interpolation.

7.2.3 | Materials

PF-3845 (*N*-3-pyridinyl-4-[[3-[[5-(trifluoromethyl)-2-pyridinyl]-oxy]phenyl]methyl]-1-piperidinecarboxamide) was purchased from Tocris Bioscience (R&D Systems Europe Ltd., Abingdon, UK). Deuterated NAEs were synthesized in the laboratory of Prof. Muccioli following well-established procedures.

7.3 | Docking

A model of the mouse FAAH was built, using SWISSMODEL, by homology with the crystal structure of the humanised-rat FAAH (pdb code:2VYA), as a template. Docking of the inhibitors into the active site of the mouse FAAH was performed using GOLD. It is based on a genetic algorithm (GA), performing docking of flexible ligands into proteins with partial flexibility in the neighbourhood of the active site [20]. The binding region was defined as a 17 Å radius sphere centred on Leu_{192}. For the 20 GA runs performed, a total of 100 000 genetic operations were carried out on 5 islands, each containing 100 individuals. The solutions were ranked by the GOLD score. The GOLD fitness function is made up of four components: protein-ligand hydrogen bond energy, protein-ligand van der Waals energy, ligand internal van der Waals energy, and ligand torsional strain energy. The figures were produced, and the H-bond lengths were calculated using PyMOL [21].

7.4 | Statistical Analysis

The data shown represent the mean ± SD of three independent experiments.

Author Contributions

Axel Morelle: conduction of experiments for synthesis and pharmacological assessment, data analysis, writing, and coordination. **Juhans Dechenne**: conduction of experiments for synthesis, data analysis, and writing. **Joséphine Caruano**: conduction of experiments for synthesis and pharmacological assessment, data analysis, and writing. **Olivia Vander Auwera**: conduction of experiments for synthesis, data analysis, and writing. **Gabriella Barozzino-Consiglio**: NMR analysis, writing. **Catherine Michaux**: conceptualization, docking study, writing, and funding. **Giulio G. Muccioli**: conceptualization, supervision, biochemical and pharmacological assessment, writing, and funding. **Raphaël Robiette**: conceptualization, supervision, writing, and funding.

Acknowledgments

Computational resources have been provided by the supercomputing facilities of the Université catholique de Louvain (CISM/UCL) and the Consortium des Équipements de Calcul Intensif (CÉCI) en Fédération Wallonie Bruxelles (CÉCI), funded by the Fonds de la Recherche Scientifique-FNRS (F.R.S.-FNRS) under convention 2.5020.11 and by the Walloon Region. NMR spectra, mass spectra, and high-resolution mass spectra were recorded by the ASM technological platform of UCLouvain. Catherine Michaux and Raphaël Robiette thank the FNRS for their

Senior Research Associate position. Catherine Michaux is appreciative of the PTCI high-performance computing resource. Prof Mireille Alhouayek (BPBL/LDRI/UCLouvain) is acknowledged for her help with the biochemical assays. Romano Terrasi (BPBL/LDRI/UCLouvain) is acknowledged for his help with the lipid quantification.

Funding

Computational resources have been provided by the supercomputing facilities of the Université catholique de Louvain (CISM/UCL) and the Consortium des Équipements de Calcul Intensif (CÉCI) en Fédération Wallonie Bruxelles (CÉCI), funded by the Fonds de la Recherche Scientifique-FNRS (F.R.S.-FNRS) under convention 2.5020.11 and by the Walloon Region.

Conflicts of Interest

The authors declare no conflicts of interest.

Data Availability Statement

The authors have nothing to report.

References

1. A. Romano, M. Friuli, B. Eramo, et al., ""To Brain or Not to Brain": Evaluating the Possible Direct Effects of the Satiety Factor Oleoylethanolamide in the Central Nervous System," *Frontiers in Endocrinology* 14 (2023): 1158287–1159299, https://doi.org/10.3389/fendo.2023.1158287.

2. N. van Egmond, V. M. Straub, and M. van der Stelt, "Targeting Endocannabinoid Signaling: FAAH and MAG Lipase Inhibitors," *Annual Review of Pharmacology and Toxicology* 61 (2021): 441–463.

3. J. E. Schlosburg, S. G. Kinsey, and A. H. Lichtman, "Targeting Fatty Acid Amide Hydrolase (FAAH) to Treat Pain and Inflammation," *AAPS Journal [Electronic Resource]* 11 (2009): 39–44, https://doi.org/10.1208/s12248-008-9075-y.

4. K. Ahn, D. S. Johnson, M. Mileni, et al., "Discovery and Characterization of a Highly Selective FAAH Inhibitor that Reduces Inflammatory Pain," *Chemistry & Biology* 16 (2009): 411–420, https://doi.org/10.1016/j.chembiol.2009.02.013.

5. N. R. Bachur and S. Udenfriend, "Microsomal Synthesis of Fatty Acid Amides," *Journal of Biological Chemistry* 241 (1966): 1308–1313, https://doi.org/10.1016/S0021-9258(18)96775-X.

6. M. K. McKinney and B. F. Cravatt, "Structure and Function of Fatty Acid Amide Hydrolase," *Annual Review of Biochemistry* 74 (2005): 411–432, https://doi.org/10.1146/annurev.biochem.74.082803.133450.

7. A. Minkkilä, S. M. Saario, H. Käsnänen, J. Leppänen, A. Poso, and T. Nevalainen, "Discovery of Boronic Acids as Novel and Potent Inhibitors of Fatty Acid Amide Hydrolase," *Journal of Medicinal Chemistry* 51 (2008): 7057–7060, https://doi.org/10.1021/jm801051t.

8. R. K. P. Tripathi, "A Perspective Review on Fatty Acid Amide Hydrolase (FAAH) Inhibitors as Potential Therapeutic Agents," *European Journal of Medicinal Chemistry* 188 (2020): 111953, https://doi.org/10.1016/j.ejmech.2019.111953.

9. M. Mileni, S. Kamtekar, D. C. Wood, T. E. Benson, B. F. Cravatt, and R. C. Stevens, "Crystal Structure of Fatty Acid Amide Hydrolase Bound to the Carbamate Inhibitor URB597: Discovery of a Deacylating Water Molecule and Insight Into Enzyme Inactivation," *Journal of Molecular Biology* 400 (2010): 743–754, https://doi.org/10.1016/j.jmb.2010.05.034.

10. D. Piomelli, G. Tarzia, A. Duranti, et al., "Pharmacological Profile of the Selective FAAH Inhibitor KDS-4103 (URB597)," *CNS Drug Reviews* 12 (2006): 21–38, https://doi.org/10.1111/j.1527-3458.2006.00021.x.

11. D. S. Johnson, C. Stiff, S. E. Lazerwith, et al., "Discovery of PF-04457845: A Highly Potent, Orally Bioavailable, and Selective Urea FAAH Inhibitor," *ACS Medicinal Chemistry Letters* 2 (2011): 91–96, https://doi.org/10.1021/ml100190t.

12. M. Feledziak, G. G. Muccioli, D. M. Lambert, and J. Marchand-Brynaert, "SAR and LC/MS Studies of β-Lactamic Inhibitors of Human Fatty Acid Amide Hydrolase (h FAAH): Evidence of a Nonhydrolytic Process," *Journal of Medicinal Chemistry* 54 (2011): 6812–6823, https://doi.org/10.1021/jm200723m.

13. M. Feledziak, C. Michaux, D. M. Lambert, and J. Marchand-Brynaert, "An unprecedented reversible mode of action of β-lactams for the inhibition of human fatty acid amide hydrolase (hFAAH)," *European Journal of Medicinal Chemistry* 60 (2013): 101–111, https://doi.org/10.1016/j.ejmech.2012.11.035.

14. M. Feledziak, C. Michaux, A. Urbach, et al., "β-Lactams Derived From a Carbapenem Chiron Are Selective Inhibitors of Human Fatty Acid Amide Hydrolase versus Human Monoacylglycerol Lipase," *Journal of Medicinal Chemistry* 52 (2009): 7054–7068, https://doi.org/10.1021/jm9008532.

15. C. Walsh, "Suicide Substrates: Mechanism-based Enzyme Inactivators," *Tetrahedron* 38 (1982): 871–909, https://doi.org/10.1016/0040-4020(82)85068-0.

16. J. Caruano, M. Feledziak, G. Labar, et al., "(S)-1-(Pent-4′-enoyl)-4-(hydroxymethyl)-azetidin-2-one Derivatives as Inhibitors of Human Fatty Acid Amide Hydrolase (h FAAH): Synthesis, Biological Evaluation and Molecular Modelling," *Journal of Enzyme Inhibition and Medicinal Chemistry* 29 (2014): 654–662, https://doi.org/10.3109/14756366.2013.837900.

17. Y. Kozawa and M. Mori, "Novel Synthesis of Carbapenam by Intramolecular Attack of Lactam Nitrogen Toward η 1 -Allenyl and η 3 -Propargylpalladium Complex," *Journal of Organic Chemistry* 68 (2003): 8068–8074, https://doi.org/10.1021/jo030123c.

18. D. Leung, C. Hardouin, D. L. Boger, and B. F. Cravatt, "Discovering potent and selective reversible inhibitors of enzymes in complex proteomes," *Nature Biotechnology* 21 (2003): 687–691, https://doi.org/10.1038/nbt826.

19. M. Alhouayek, P. Bottemanne, A. Makriyannis, and G. G. Muccioli, "N -acylethanolamine-hydrolyzing acid amidase and fatty acid amide hydrolase inhibition differentially affect N -acylethanolamine levels and macrophage activation," *Biochimica Et Biophysica Acta* 1862 (2017): 474–484, https://doi.org/10.1016/j.bbalip.2017.01.001.

20. G. Jones, P. Willett, R. C. Glen, A. R. Leach, and R. Taylor, "Development and Validation of a Genetic Algorithm for Flexible Docking[1]: [1]Edited by F. E. Cohen," *Journal of Molecular Biology* 267 (1997): 727–748, https://doi.org/10.1006/jmbi.1996.0897.

21. *The PyMOL Molecular Graphics System*, *Version 3.0.2, Schrödinger, LLC*.

22. P. Galletti, A. Quintavalla, C. Ventrici, et al., "Azetidinones as Zinc-Binding Groups to Design Selective HDAC8 Inhibitors," *ChemMedChem* 4 (2009): 1991–2001, https://doi.org/10.1002/cmdc.200900309.

23. J. T. Drummond and G. Johnson, "Synthesis of a cognition enhancing beta-lactam fused gamma-lactam," *Tetrahedron Letters* 28 (1987): 5245–5248, https://doi.org/10.1016/S0040-4039(00)96698-X.

24. S.-K. Kang, T.-G. Baik, X.-H. Jiao, K.-J. Lee, and C. H. Lee, "Indium-mediated Substitution of 4-Acetoxy-2-azetidinones: Synthesis of 4-Allyl-2-azetidinones," *Synlett* 1999 (1999): 447–449, https://doi.org/10.1055/s-1999-2652.

25. M. E. Geherty, "Catalytic Asymmetric Claisen Rearrangements. The Development of Ru(II)-Catalyzed Formal [3,3] Sigmatropic Rearrangements and Related Enolate Allylation Reactions." (PhD Dis., University of Pittsburgh, 2012).

26. T. Tsuda, H. Satomi, T. Hayashi, and T. Saegusa, "Alkylation and Silylation of the Aluminum Enolates Generated by Hydroalumination of Alpha, Beta-Unsaturated Carbonyl Compounds," *Journal of Organic Chemistry* 52 (1987): 439–443, https://doi.org/10.1021/jo00379a024.

27. G. G. Muccioli, C. Xu, E. Odah, et al., "Identification of a Novel Endocannabinoid-Hydrolyzing Enzyme Expressed by Microglial Cells," *Journal of Neuroscience* 27 (2007): 2883–2889, https://doi.org/10.1523/JNEUROSCI.4830-06.2007.

28. *Jaguar 8.5, Schrodinger, Inc., New York, NY* (2014).

29. A. D. Becke, "Density-functional thermochemistry. III. The role of exact exchange," *Journal of Chemical Physics* 98 (1993): 5648–5652, https://doi.org/10.1063/1.464913.

30. P. J. Stephens, F. J. Devlin, C. F. Chabalowski, and M. J. Frisch, "Ab Initio Calculation of Vibrational Absorption and Circular Dichroism Spectra Using Density Functional Force Fields," *Journal of Chemical Physics* 98 (1994): 11623–11627, https://doi.org/10.1021/j100096a001.

31. S. Grimme, J. Antony, S. Ehrlich, and H. Krieg, "A consistent and accurate ab initio parametrization of density functional dispersion correction (DFT-D) for the 94 elements H-Pu," *Journal of Chemical Physics* 132 (2010): 154104.

Supporting Information

Additional supporting information can be found online in the Supporting Information section.

The authors have cited additional references within the Supporting Information [22–31].